Atmos. Chem. Phys., 13, 6263–6274, 2013
www.atmos-chem-phys.net/13/6263/2013/
doi:10.5194/acp-13-6263-2013

Atmospheric Chemistry and Physics Open Access

Atmospheric test of the $J(BrONO_2)/k_{BrO+NO_2}$ ratio: implications for total stratospheric Br_y and bromine-mediated ozone loss

S. Kreycy[1], C. Camy-Peyret[2], M. P. Chipperfield[3], M. Dorf[1], W. Feng[4], R. Hossaini[3], L. Kritten[5], B. Werner[1], and K. Pfeilsticker[1]

[1]Institute of Environmental Physics, University of Heidelberg, Heidelberg, Germany
[2]Laboratoire de Physique Moléculaire pour l'Atmosphère et l'Astrophysique (LPMAA), Université Pierre et Marie Curie, Paris, France
[3]Institute for Climate and Atmospheric Science, School of Earth and Environment, University of Leeds, Leeds, UK
[4]National Centre for Atmospheric Science, School of Earth and Environment, University of Leeds, Leeds, UK
[5]Institute for Space Sciences, Free University Berlin, Berlin, Germany

Correspondence to: K. Pfeilsticker (klaus.pfeilsticker@iup.uni-heidelberg.de)

Received: 26 September 2012 – Published in Atmos. Chem. Phys. Discuss.: 23 October 2012
Revised: 30 April 2013 – Accepted: 2 June 2013 – Published: 2 July 2013

Abstract. We report on time-dependent O_3, NO_2 and BrO profiles measured by limb observations of scattered skylight in the stratosphere over Kiruna (67.9° N, 22.1° E) on 7 and 8 September 2009 during the autumn circulation turn-over. The observations are complemented by simultaneous direct solar occultation measurements around sunset and sunrise performed aboard the same stratospheric balloon payload. Supporting radiative transfer and photochemical modelling indicate that the measurements can be used to constrain the ratio $J(BrONO_2)/k_{BrO+NO_2}$, for which at $T = 220 \pm 5$ K an overall $1.7(+0.4-0.2)$ larger ratio is found than recommended by the most recent Jet Propulsion Laboratory (JPL) compilation (Sander et al., 2011). Sensitivity studies reveal the major reasons are likely to be (1) a larger $BrONO_2$ absorption cross-section σ_{BrONO_2}, primarily for wavelengths larger than 300 nm, and (2) a smaller k_{BrO+NO_2} at 220 K than given by Sander et al. (2011). Other factors, e.g. the actinic flux and quantum yield for the dissociation of $BrONO_2$, can be ruled out.

The observations also have consequences for total inorganic stratospheric bromine (Br_y) estimated from stratospheric BrO measurements at high NO_x loadings, since the ratio $J(BrONO_2)/k_{BrO+NO_2}$ largely determines the stratospheric BrO/Br_y ratio during daylight. Using the revised $J(BrONO_2)/k_{BrO+NO_2}$ ratio, total stratospheric Br_y is likely to be 1.4 ppt smaller than previously estimated from BrO profile measurements at high NO_x loadings. This would bring estimates of Br_y inferred from organic source gas measurements (e.g. CH_3Br, the halons, CH_2Br_2, $CHBr_3$, etc.) into closer agreement with estimates based on BrO observations (inorganic method). The consequences for stratospheric ozone due to the revised $J(BrONO_2)/k_{BrO+NO_2}$ ratio are small (maximum -0.8 %), since at high NO_x (for which most Br_y assessments are made) the enhanced ozone loss by overestimating Br_y is compensated for by the suppressed ozone loss due to the underestimation of BrO/Br_y with a smaller $J(BrONO_2)/k_{BrO+NO_2}$ ratio.

1 Introduction

The effect reactive bromine has on stratospheric ozone is largely dominated by the Reactions (1), (2a), and (2b) (Spencer and Rowland, 1977):

$$BrO + NO_2 + M \longrightarrow BrONO_2 + M \quad \text{(R1)}$$

$$BrONO_2 + h \cdot \nu \longrightarrow BrO + NO_2 \ (0.15) \quad \text{(R2a)}$$

$$BrONO_2 + h \cdot \nu \longrightarrow Br + NO_3 \ (0.85). \quad \text{(R2b)}$$

The brackets give the recommended quantum yields Φ for $\lambda > 300$ nm. They determine the amount of reactive bromine (BrO) and thus the bromine-mediated ozone loss in almost the whole global lower stratosphere during daytime, except

in the chlorine-activated polar ozone hole regions. Sander et al. (2011) report for the termolecular Reaction (1) a 1σ uncertainty factor of 1.47 (at 220 K) and for the $BrONO_2$ absorption cross-section, $\sigma(BrONO_2)$ (Reactions 2a and 2b) and hence for $J(BrONO_2)$ an overall uncertainty factor of at least 1.4 (e.g. taken from Table 4.2 in JPL-2011). The former uncertainty factor mostly arises from the extrapolation of the laboratory measurements of k_{BrO+NO_2} from high to low temperatures. The uncertainty of $\sigma(BrONO_2)$ is due to its large decrease by 3.5 orders of magnitude with wavelength, when going from the extreme UV ($\lambda = 200$ nm) to $\lambda > 300$ nm, where the actinic fluxes, and thus the spectral contribution to $J(BrONO_2)$, strongly increase.

$BrONO_2$ can also be destroyed by the reaction (Soller et al., 2002)

$$BrONO_2 + O(^3P) \longrightarrow BrO + NO_3. \quad \text{(R3)}$$

Nevertheless, Reaction (3) has a negligible effect on the lifetime of $BrONO_2$ below about 25 km (Sinnhuber et al., 2005), where the bulk of $BrONO_2$ resides during our measurements.

2 Methods

We report on spectroscopic measurements taken during a balloon flight of the LPMA/DOAS (Limb Profile Monitor of the Atmosphere/Differential Optical Absorption Spectroscopy) payload at Kiruna, Sweden (67.9° N, 22.1° E), on 7 and 8 September 2009. The payload accommodated three spectrometers: (a) a near-IR (LPMA) spectrometer that is suitable for the detection of O_3, NO_2, CH_4, N_2O, HNO_3, and other trace-gases (e.g. Camy-Peyret et al., 1995; Payan et al., 1998); (b) a UV/vis spectrometer for the high-precision detection of O_3, NO_2, BrO, IO, O_4, etc. in direct sunlight (e.g. Harder et al., 1998; Ferlemann et al., 2000); and (c) a UV/vis mini-DOAS instrument primarily for the detection of O_3, NO_2, and BrO in limb-scattered skylight (e.g. Weidner et al., 2005; Kritten et al., 2010).

While spectrometers (a) and (b) measured direct sunlight during balloon ascent, solar occultation at sunset and sunrise, the mini-DOAS instrument recorded the atmosphere in limb geometry, with the azimuth angle being clockwise perpendicular ($\alpha = 90°$) to the sun's azimuth direction. Viewing elevation angles were held constant ($+0.05°$) during balloon ascent but subsequently changed from $+0.6°$ to $-4.88°$ elevation angle in steps of 0.39° for the limb observations at balloon float altitude.

The balloon was launched at 14:50 UT at a solar zenith angle (SZA) of 75° on 7 September 2009, and balloon float altitude (≈ 33.5 km) was reached around 16:45 UT (SZA = 86°). Please note that here and in the following all SZAs refer to local SZA (i.e. for the balloon gondola position). On 7 September 2009 the solar occultation and limb observations during sunset lasted until 18:15 UT (SZA = 94°), and were resumed at 02:30 UT during sunrise on 8 September 2009 (SZA = 94°). However, the scanning motor of the limb observation spectrometer malfunctioned, and only spectra recorded after 03:50 UT (SZA = 86°) are used for analysis. They lasted until 06:00 UT (SZA = 75°), when the payload was separated from the balloon. Due to the low stratospheric winds at high latitudes during summer/winter circulation turn-over, the balloon payload gently drifted from Kiruna to the Finnish–Russian border (at around 350 km distance) within the 16 h long flight. Accordingly, due to the low shear winds the azimuth stabilisation of the balloon gondola, and therefore the sun and limb pointing, was extremely stable as compared to previous balloon flights (e.g. see Table 1 in Dorf et al., 2006a; Kritten et al., 2010). Further, the ambient temperature ($T = 220$ K) did not change by more than ± 5 K within the altitude range from 11.5 to 31 km.

Here we primarily report on the DOAS data obtained from the limb observations during sunset and sunrise and data recorded during sunset using the direct sunlight spectrometer.

For both instruments the spectral retrieval is based on the DOAS method (Platt and Stutz, 2008). Since in previous studies the spectral retrieval has been described at length (e.g. Weidner et al., 2005; Dorf et al., 2006a; Butz et al., 2006; Kritten et al., 2010), here only those details are described which depart from our previous work. The retrieval of O_3, NO_2, and BrO from the solar occultation and the mini-DOAS measurements is performed along the parameters as given in Butz et al. (2006) and Aliwell et al. (2002), with updates as recently described in Dorf et al. (2008) and Kritten et al. (2010). Also, since the errors and uncertainties of the DOAS retrievals have already been discussed in length in previous studies (e.g. Harder et al., 1998; Aliwell et al., 2002; Weidner et al., 2005; Dorf et al., 2006a; Butz et al., 2006), they are only referred to when necessary. The results of the DOAS analysis are differential slant column densities (dSCDs) with respect to a reference spectrum, typically recorded directly after reaching balloon float altitude at low SZA (see Fig. 1). These values are then corrected for the amount of the targeted trace gas in the reference spectrum resulting in absolute slant column densities (SCDs).

The limb radiances are modelled using version 2.1 of the Monte Carlo radiative transfer (RT) model McArtim (Deutschmann et al., 2011). The model's input is chosen according to measured atmospheric temperatures and pressures, including a climatological high-latitude summer aerosol profile inferred from SAGE III (https://eosweb.larc.nasa.gov/project/sage3/sage3_table) and confirmed with the direct sun measurement of spectrometer (b) (Gurlit et al., 2005), the balloon altitude and the geolocation, SZAs as encountered during each measurement, the azimuth and elevation angles, as well as the field of view (FOV) of the mini-DOAS telescopes. Since the mini-DOAS spectrometer is not absolutely radio-metrically calibrated, all simulations are performed relative to the first limb spectrum (elevation

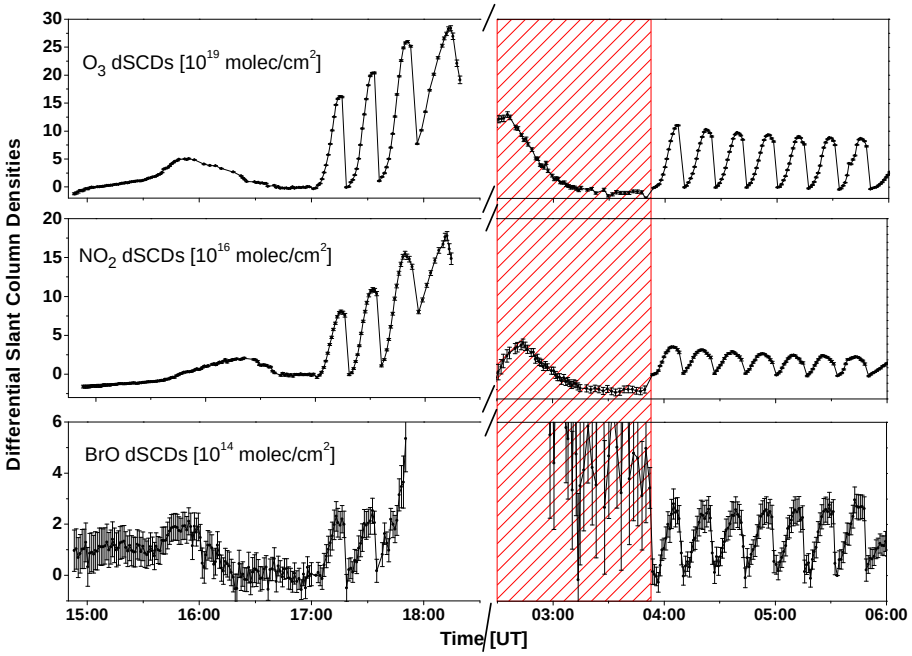

Fig. 1. Measured differential slant column densities of O_3 (upper panel), NO_2 (middle panel), and BrO (lower panel) in limb geometry during the balloon flight from Kiruna on 7 and 8 September 2009. During balloon ascent from 14:50 UT until 17:10 UT, the limb radiation was observed for an elevation angle of 0.05°. During dusk (17:10 to 18:30 UT), 3.5 limb scans were performed at 33 km altitude. During early dawn, the scanning telescope of the limb spectrometer malfunctioned (the reddish area), and the limb scans (in total 7.25) started at 03:50 UT and continued until 06:00 UT, when the balloon was floating at 31 km altitude. Each limb scan consists of limb observations from $+0.6°$ elevation angle down to $-4.88°$ in steps of 0.39°.

angle $+0.6°$) of each limb sequence. It is noteworthy that the radiometric calibration does not change between the individual limb sequences, except for very high SZAs $> 93°$, when spectrometer stray light becomes important. This finding is in agreement with the small mismatch between measured and modelled limb radiances also found by Deutschmann et al. (2011) (see Figures 5 and 6 therein). Figure 2 indicates how well the modelled and measured relative radiances are reproduced for the limb observations at $\lambda = 350$, 450, and 495 nm, where BrO, NO_2 and O_3 are evaluated, respectively. The good agreement indicates that both the relevant observation parameters (e.g. balloon altitude, SZA, elevation and azimuth angles, FOV) and the atmospheric parameters (T, p, aerosol concentration, and their optical properties, as well as the low level cloud cover (about 2/8)) are well represented in the RT model.

For the interpretation of the direct sun observations, our group's ray-tracing model (DAMF) is used that was extensively tested in the profile retrievals of past balloon flights (e.g. Harder et al., 2000, see Figure 1 therein).

For the photochemical modelling, the output from the most recent simulations of the 3-D CTM SLIMCAT (Chipperfield, 1999) at Kiruna for 6 September 2009 is used to initialise our 1-D facsimile code Labmos (e.g. Bösch et al., 2003). This approach is necessary here since the output from a global SLIMCAT run is only available every 48 h. This time resolution is too coarse to be used for comparisons with measurements. On the other hand using a 1-D photochemical model for the model versus measurement intercomparison appears justified, since during the balloon flight stratospheric winds were low, and thus very likely the same air masses were probed throughout our observations. However, both photochemical models use the most recent version of the Jet Propulsion Laboratory (JPL) kinetics and thermochemical data for all relevant gas-phase and heterogeneous reactions (Sander et al., 2011). Finally, the Labmos simulations are constrained to the measured N_2O and CH_4 from spectrometer (a) to correct for small mismatches in the profiles of the source gases due to a small bias in the diabatic heating rate of SLIMCAT. Total stratospheric bromine (Br_y) is set to 20.3 ppt, and the Br_y mixing ratio profile is accordingly vertically shifted (about 2 km) until the modelled and measured N_2O and CH_4 profiles match. For this flight [Br_y] was (20.3±2.5) ppt (presumably in 5 yr-old air), which is determined from the direct sun measurements at balloon float using the so-called Langley method (e.g. Dorf et al., 2006b, 2008). Also note that, for the assessment of Br_y using Langley's method, stratospheric BrO is probed above balloon float, where the BrO/Br_y partitioning is mostly due to Br atoms and BrO, and thus is insensitive to $J(BrONO_2)$ and/or k_{BrO+NO_2}. The initialisation is further constrained to O_3 and

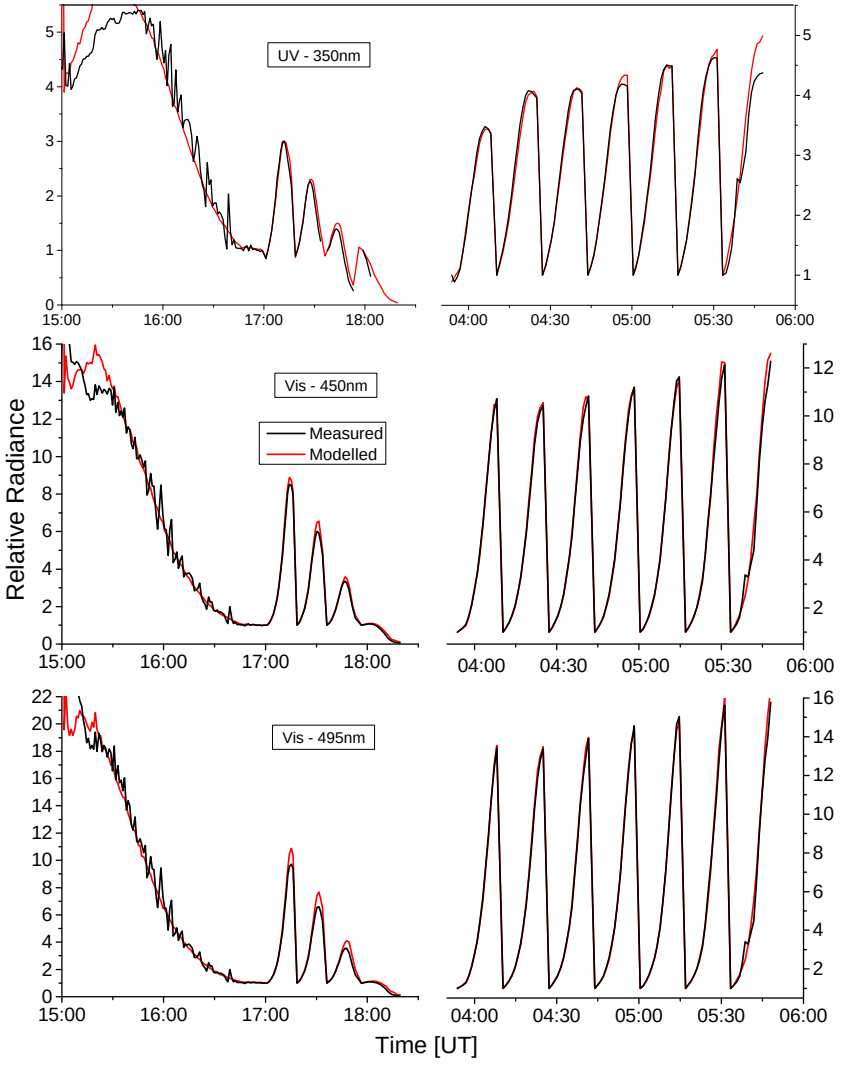

Fig. 2. Inter-comparison of measured (black) and modelled (red) relative radiances at $\lambda = 350$, 450, and 495 nm for the limb scans as described in the legend of Fig. 1. The RT simulations are normalised for the balloon ascent to the observations at 17:00 UT, and for each limb scan to the observation for the largest elevation angle (0.6°), i.e. for the lowest radiances.

NO_2 obtained from the direct sun observations of spectrometer (b) (see Fig. 4).

As an example of the simulations, Fig. 3 shows the simulated 2-D fields of BrO, $BrONO_2$, and HOBr over Kiruna for 7 and 8 September 2009. Here, the simulation indicates that balloon soundings are well suited to study the Reactions (1), (2a), and (2b) at northern high latitudes during the summer to winter circulation turn-over, mostly because NO_x concentrations are large and the profiles of both targeted gases (NO_2, and BrO) nicely overlap as well, thus providing a good sensitivity for Reaction (1) during sunset.

At early dawn, unlike at dusk the Br_y partitioning (the period of the red dashed lines in Fig. 3), is largely given by the efficiency of the heterogenous reaction of

$$BrONO_2 + H_2O|_{aqueous} \longrightarrow HOBr + HNO_3 \qquad (R4)$$

at night. This is mostly because (a) Reaction (4) is much slower than Reaction (1) in the volcanically quiet stratosphere, and (b) the photolysis of HOBr is similarly rapid as for $BrONO_2$ (Erle et al., 1999) (see also Fig. 3). Therefore, HOBr does not interfere with our measurements, except for the solar occultation measurements during early sunrise, which are not considered any further here. They will be discussed in a separate study addressing the stratospheric HOBr photochemistry.

In order to support an inter-comparison of measured and modelled SCDs of O_3, NO_2 and BrO, the simulated photochemical fields are fed into the RT models McArtim and DAMF, where path integrals through the simulated photochemical fields are calculated and then compared with the measured SCDs.

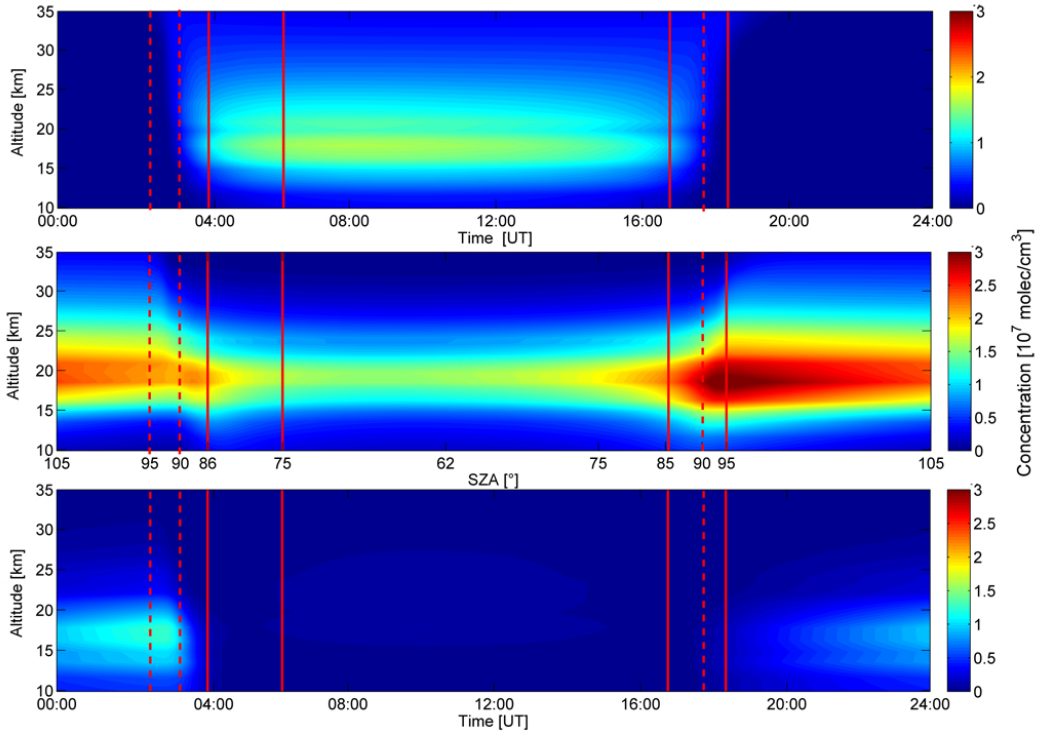

Fig. 3. Standard simulation of the key stratospheric bromine species for 7 September 2009 using the Labmos photochemical model: diurnal variation of BrO (upper panel), $BrONO_2$ (middle panel), and HOBr (lower panel). The red lines indicate the periods of the limb measurements (local SZA at the balloon gondola = 86–75° at a.m. and 85–95° at p.m.) and the dashed red lines the period of the direct sunlight measurements (local SZA = 95–90° at a.m., and SZA = 90–95° at p.m.). Solar zenith angles shown in the middle panel refer to the SZA at the balloon location, and the colour coding indicates the respective concentrations in units of 10^7 molec cm^{-3}.

3 Results

Figure 4 displays the inter-comparison of the measured and modelled limb SCDs of O_3, NO_2 and BrO. While for O_3 and NO_2 the agreement is naturally close to perfect for all elevation angles due to the scaling of the profiles, measured limb BrO is in general larger than obtained from the simulations for the standard run (i.e. $[Br_y] = 20.3$ ppt, $\sigma(BrONO_2)$ and k_{BrO+NO_2} from JPL-2011). This is in particular true for the large BrO SCDs, which are obtained for large negative elevation angles (tangent heights down to 14 km), where the bulk of BrO and $BrONO_2$ resides. In short, our observations indicate that during dusk BrO tends to react later (or at larger SZAs) into its major night-time reservoir gas $BrONO_2$, while at dawn (SZA < 86°) limb BrO tends to appear more rapidly than the standard simulation suggests.

A similar finding is obtained from the solar occultation measurements during sunset (see Fig. 5, upper panel) using the direct sun instrument (b) (Ferlemann et al., 2000) even though they are less sensitive to Reactions (2a) and (2b). This is mostly since the tangent height is by definition at SZA = 90° where most of the absorption signal comes from. Hence, our solar occultation observations mostly probe the atmosphere for a more-or-less constant $J(BrONO_2)$, but at the same time the effectively probed air masses (i.e. tangent points) move more and more away from the payload (up to 1200 km), towards the northwest during sunset.

Noteworthy in the comparison of measured and modelled BrO SCDs is the kink observed in the measurements for SZAs > 92.5°, or tangent heights lower than 25.5 km. It is suspected that this kink is due to a dynamically different lowermost stratosphere close to and distant to the balloon sounding, rather than due to deficits in modelling the photochemistry of BrO. Two pieces of evidence support this hypothesis. First, a similar kink for the same SZA occurs in the measured O_3 SCDs (see Fig. 5, lower panel), which requires the inferred profiles of O_3 close to and distant to the sounding to be distinctly different for tangent heights lower than 25.5 km (see the insets in the lower panel of Fig. 5). Accordingly, since in the lowermost stratosphere at high latitudes the profile shape of O_3 is mostly due to dynamical processes (i.e. quasi-isentropic exchange of air masses with mid-latitudes, or the height of the tropopause), it is also suspected that the profile shape of Br_y and hence BrO is distinctly different close to and distant to the sounding. Furthermore, an inspection of the assimilation maps of the MIMOSA model's (http://ether.ipsl.jussieu.fr/ether/pubipsl/mimosa_2009_uk.jsp) potential vorticity (PV)

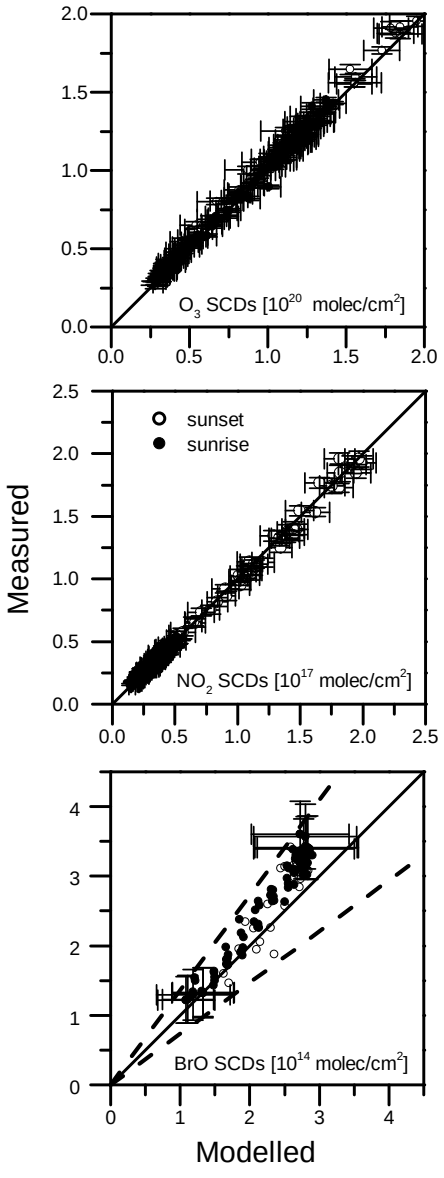

Fig. 4. Inter-comparison of limb measured versus modelled slant column concentrations of O_3 (upper panel), NO_2 (middle panel) and BrO (lower panel) for the standard JPL-2011 kinetics in units as given in the panels. Due to the scaling the slant column densities of O_3 and NO_2 excellently agree, but only fair agreement is obtained for BrO with standard model parameters. In the lower panel the JPL-2011 uncertainty of the $J(BrONO_2)/k_{BrO+NO_2}$ ratio is indicated (dashed lines).

indicates a negligible PV gradient at the upper level (950 K), and a small west/east PV gradient at the lower levels (at 475 K and 550 K), again indicative of different origins of the air masses close to and distant to the balloon sounding. Therefore, it is rather likely that the kink of the measured BrO SCD at around SZA = 92.5° is not due to photochemistry, but due to transport. Therefore, the solar occultation measurements during dusk for SZAs > 92.5° are disregarded for the following discussion.

Accordingly, the findings inferred from the comparisons of the limb and solar occultation measurements with the photochemical modelling can be taken as evidence that either the ratio $J(BrONO_2)/k_{BrO+NO_2}$ is larger than indicated by the JPL-2011 compilations, or that Br_y is incorrectly assumed in the model. These possibilities are investigated in the following section.

4 Discussion

In order to investigate potential causes for the deviation of the measured versus modelled BrO SCDs, a sensitivity test for the magnitude of the parameters $J(BrONO_2)$, k_{BrO+NO_2}, and Br_y is performed for limb and solar occultation measurements (Figs. 6 and 7). In both cases the best agreement between measurements and simulations is found by increasing $J(BrONO_2)$ and decreasing k_{BrO+NO_2}, when forcing the regression line of measured versus modelled BrO SCDs through 0. Figure 8 illustrates the situation when varying $J(BrONO_2)$ and k_{BrO+NO_2} for both the limb (dusk and dawn) and the solar occultation measurements (dusk), whereby the colour coding denotes the slope of the regression of measured versus modelled BrO SCDs. The figure indicates that for the limb measurement the best combination of $J(BrONO_2)$, and k_{BrO+NO_2} is obtained when increasing $J(BrONO_2)$ to a range of 1.1 to 1.4 and decreasing k_{BrO+NO_2} to a range of 0.65 to 0.80. RT calculations show that the limb samples are taken 30–70 km on the right-hand side of the payload, while the probed air masses of the solar occultation measurements move further and further away (up to 1200 km) as the sun sets.

The best agreement for the limb observations is found for a ratio $J(BrONO_2)/k_{BrO+NO_2}|_{obs} = 1.7(+0.4-0.2) \times J(BrONO_2)/k_{BrO+NO_2}|_{JPL}$, for both the sunset and sunrise measurements.

For the solar occultation observations, the comparison between measured and modelled SCDs fully supports this conclusion, however, only for SZA < 92.5°. For the solar occultation observations, the best agreement is obtained for a ratio of $J(BrONO_2)/k_{BrO+NO_2}|_{obs} = 1.7(+0.2-0.1)$. Here the uncertainties are smaller compared to the limb observations, when varying the $J(BrONO_2)/k_{BrO+NO_2}$ ratio within the errors of the slope due to the higher accuracy of calculating the RT. However, since the direct sunlight observations are less sensitive to Reactions (2a) and (2b), these results are only used to confirm the results of the limb observations.

Sensitivity runs for $[Br_y]$ within the given uncertainty range (corresponding to ±2.5 ppt of Br_y) are also performed (not shown). Proportionally increasing/decreasing the modelled BrO SCDs by ±12.5 % (±2.5 ppt) slightly decreases/increases the slope of the data, but not far enough to

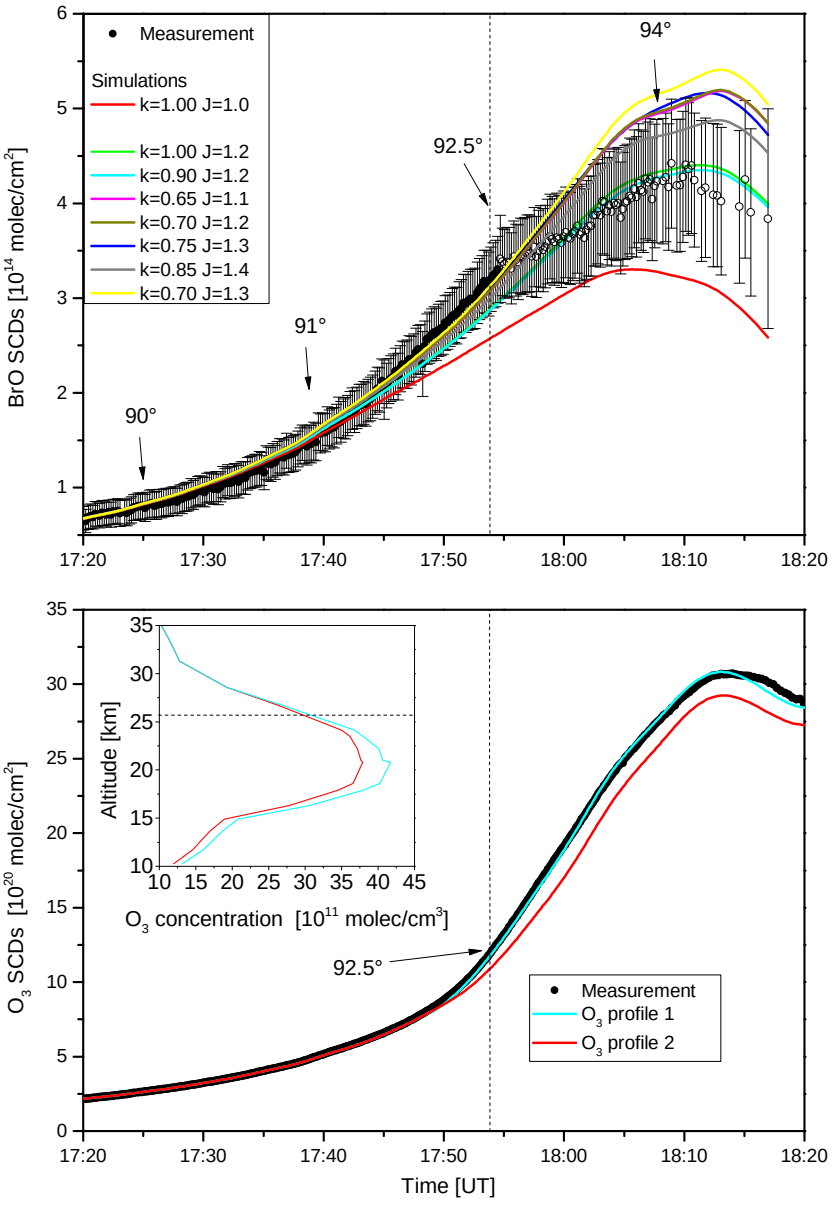

Fig. 5. Inter-comparison of measured versus modelled slant column densities of BrO (upper panel) and O_3 (lower panel) for the sunset solar occultation measurements on 7 September 2009. The data points shown with filled black dots are included, while the data points with open dots are disregarded in the analysis. The coloured lines in the upper panel show simulations for different pairs of $J(BrONO_2)$ and k_{BrO+NO_2} as indicated by the legend. Local solar zenith angles (e.g. 90°, 91°, 92.5°, and 94°) of some measurements are also indicated. The lower panel shows the measured O_3 SCDs in solar occultation, and the lines in red and light blue show the modelled O_3 SCDs for the two ozone profiles shown in the inset, respectively. The ozone profile (red line) is inferred from direct sunlight measurements in the visible spectral range during the balloon ascent (i.e. close to balloon sounding) and the ozone profile in light blue is a tuned profile to fit best the O_3 SCDs for SZA $>$ 92.5°.

obtain a 1 : 1 agreement between the modelled and measured BrO SCDs (Figs. 6 and 7).

Next, we address potential causes for the uncertainty in the $J(BrONO_2)/k_{BrO+NO_2}$ ratio. Incorrectly modelled actinic fluxes by the required amount are rather unlikely, since our RT model nicely explains the measured limb radiances at different wavelengths, different elevation angles and SZAs (e.g. see Figure 2 in Bösch et al., 2001 and Figure 5 in Deutschmann et al., 2011). Also the largely dominant contribution of the direct solar irradiance to the actinic flux seems to be well understood (e.g. Bösch et al., 2001; Gurlit et al., 2005). Moreover, since our measurement is insensitive to the quantum yields (Φ) of Reactions (2a) and (2b) (the Br atoms formed in Reaction (2b) would readily react with O_3

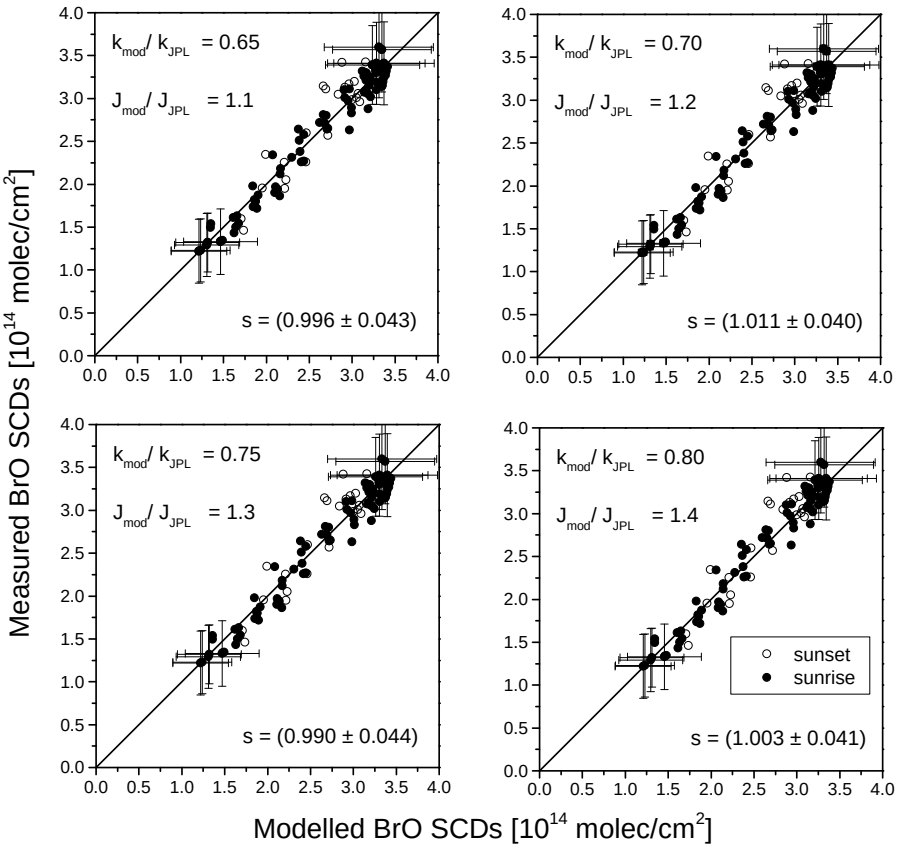

Fig. 6. Inter-comparison of limb measured versus modelled slant column densities of BrO for different scaling factors of $J(BrONO_2)$ and k_{BrO+NO_2} as indicated in the individual panels. The open dots are for sunset and the full dots for sunrise observations. The *s* value indicates the slope and its uncertainty between modelled and measured BrO SCDs.

to form BrO), an incorrect $J(BrONO_2)$ points to an incorrect $\sigma(BrONO_2)$. For $J(BrONO_2)$ JPL-2011 states an overall uncertainty factor of 1.4 (Table 4.2) most likely due to uncertainties of $\sigma(BrONO_2)$ in the UV-A and visible, and its temperature dependence. Since at $T = 298\,K$ $\sigma(BrONO_2)$ agrees fairly well among the different studies, one may speculate whether the recommended temperature correction for $T = 220\,K$ at which our measurements are made is in fact too strong. Furthermore, JPL-2011 states a 1σ uncertainty factor of 1.47 for k_{BrO+NO_2} at 220 K. Here, the major uncertainty arises from the T dependence of the high pressure limit of the reaction, which is found to be rather large ($m = 2.9$). Attempts to fit the data with the JPL master equation were found to be insufficient at low pressures (Sander et al., 2011). Therefore, one may again speculate as to whether k_{BrO+NO_2} at 220 K is somewhat lower than recommended by JPL-2011. We note while our finding requires that $J(BrONO_2)$ is larger and k_{BrO+NO_2} is lower than recommended by JPL-2011, such that $J(BrONO_2)/k_{BrO+NO_2}$=1.7(+0.4−0.2), we cannot individually assess the magnitude of each of the involved parameters. However, it is likely that, with respect to the given error bars for each parameter, both parameters need to be changed from recommended values at low temperatures.

The finding has also implications for total stratospheric bromine. Using the inorganic method to assess stratospheric Br_y relies on a photochemical correction: Br_y is calculated from measured BrO according to $[Br_y]=[BrO]\cdot(1 + k_{BrO+NO_2}\cdot[NO_2]\cdot[M]/J_{BrONO_2}\ \ldots)$ where "…" indicates contributions from minor bromine species in the stratosphere (e.g. HOBr, Br, BrCl, and HBr). In our case, taking the revised $J(BrONO_2)/k_{BrO+NO_2}$ ratio (i.e. $1.7(+0.4-0.2)$), stratospheric Br_y may decrease by as much as 1.4 ppt. In fact, a smaller Br_y assessed using the inorganic method would tend to close the existing gap to total stratospheric bromine assessed using measurements of organic source gases. Also the potential contribution of so-called very short-lived substances (VSLSs) to stratospheric bromine would accordingly decrease. For example, while our assessment of Br_y for 4.5 year old air probed over Brazil in 2005 indicated a VSLS contribution of $[VSLS]_{inorg} = (5.2 \pm 2.5)$ ppt (Dorf et al., 2008), the organic method resulted in only $[VSLS]_{org} = (1.25 \pm 0.08)$ ppt (Laube et al., 2008). A more recent comparison indicated $[VSLS]_{inorg} = (3.5 \pm 2.5)$ ppt (inferred from

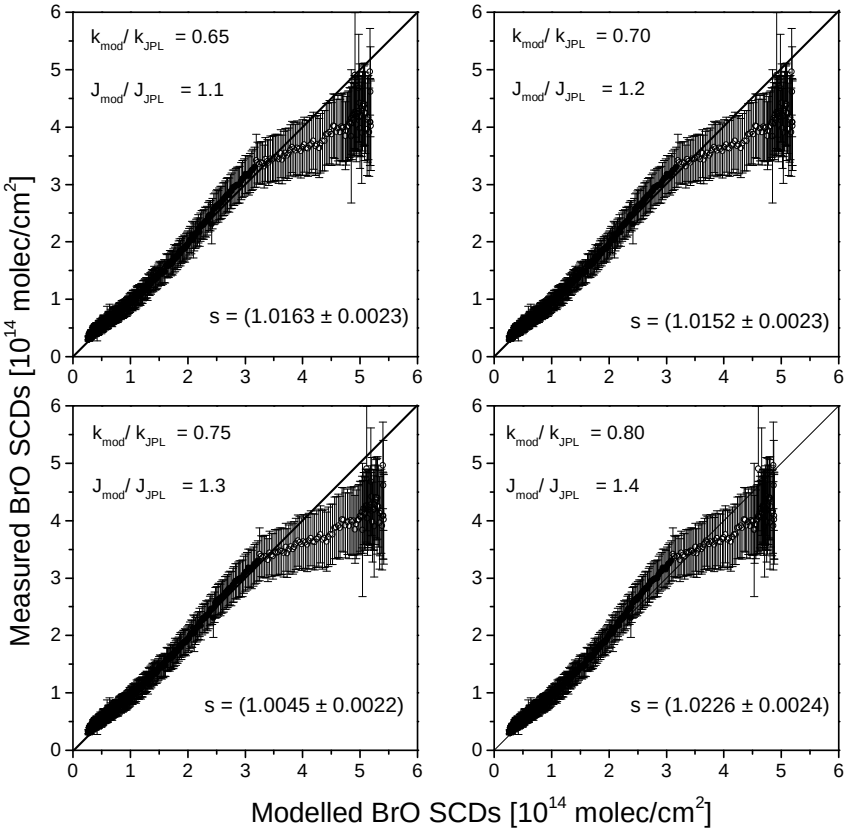

Fig. 7. Inter-comparison of solar occultation measured versus modelled slant column densities of BrO for different scaling factors of J(BrONO$_2$) and k_{BrO+NO_2} as indicated in the individual panels. The closed dots are for SZA $< 92.5°$ and the open dots for SZA $> 92.5°$, the latter being disregarded in the analysis (see text). The *s* value indicates the slope and its uncertainty between modelled and measured BrO SCDs.

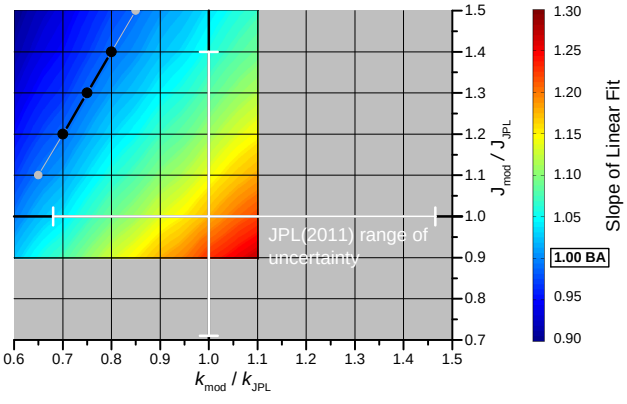

Fig. 8. Regression of J(BrONO$_2$) versus k_{BrO+NO_2} for the limb and solar occultation BrO measurements together with the uncertainty range for both parameters as indicated by the JPL-2011 compilation. The colour coding indicates the resulting slopes of the modelled versus measured BrO SCD regression of the limb and solar occultation observations, when forcing the regression line through zero. The best agreement (BA) is given for a slope of 1. The results shown in Figs. 6 and 7 are represented by the black dots.

our own BrO measurement using the Langley method) and about $[VSLS]_{org} = 2.25$ ppt (Brinckmann et al., 2012), for the air masses jointly probed by both methods over Brazil in 2008.

The implications of our finding for stratospheric ozone loss are small or even negligible, since the ozone loss by the $BrONO_2$ photolysis has a small contribution to the total ozone loss by bromine (dominated by the reaction BrO + ClO), which is presently assessed to amount to about 30–35 % on a global average (Sinnhuber et al., 2009). Furthermore, even though $BrONO_2$ mostly photolyses into Br+NO_3 (Reaction 2b), only about 12 % of the produced NO_3 photolyses into the channel NO + O_2, which in fact may cause some ozone loss (via reformation of BrO and NO_2 and the consumption of two ozone molecules). A possibly larger impact would be through the altered partitioning of bromine between BrO and its reservoir $BrONO_2$, as BrO participates in a number of ozone loss cycles.

To quantify the impact of our findings, two runs with the SLIMCAT off-line 3-D CTM are performed (e.g. Chipperfield, 2006; Feng et al., 2007). The runs are initialised in November 2008 from an existing SLIMCAT run and

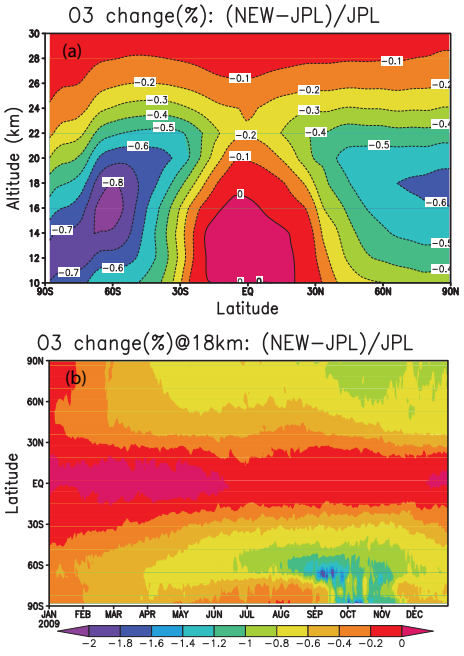

Fig. 9. Difference in ozone from a simulation of the SLIMCAT 3-D CTM with scaled J(BrONO$_2$) ($\times 1.27$) and k_{BrO+NO_2} ($\times 0.75$) compared to a run with standard JPL kinetics. **(a)** Difference (%) in annually and zonally averaged ozone and **(b)** difference (%) in zonal mean ozone at 18 km as a function of time. Note the different colour scales in the two panels.

integrated for 14 months using ECMWF meteorology. The model run has a horizontal resolution of $2.8° \times 2.8°$ and included a detailed stratospheric chemistry scheme (Chipperfield, 1999). One model run is performed with standard JPL kinetics. In the other run J(BrONO$_2$) is scaled by 1.27 and k_{BrO+NO_2} is scaled by 0.75, thereby scaling the ratio J(BrONO$_2$)/k_{BrO+NO_2} by 1.7. Figure 9 shows the percentage ozone difference between these runs for 2009 as an annual and zonal mean and as a zonal mean at 18 km altitude. Overall the impact of these kinetic changes on stratospheric ozone is small and confined to altitudes below about 30 km where BrONO$_2$ is a reservoir for bromine. The largest decrease in ozone is around 0.8 % at the edge of the Antarctic ozone region in September/October. The kinetics changes lead to less BrONO$_2$ (and HOBr) and more bromine in the form of BrO which catalyses ozone loss. The small effect itself is more important at the edge of the polar vortex and late in the season when NO_y is more readily available to form BrONO$_2$. Smaller changes are seen in the Arctic and at mid-latitudes.

In consequence, an increase in the photolysis rate and a decrease in the formation rate of BrONO$_2$ as determined here would eventually imply only a small change in the bromine-mediated ozone loss in the stratosphere.

5 Conclusions

We performed an atmospheric test of the J(BrONO$_2$)/k_{BrO+NO_2} ratio assisted by photochemical and radiative transfer modelling. It is found that, under stratospheric conditions ($T = 220 \pm 5$ K and $p \approx 65$ mbar), the ratio J(BrONO$_2$)/k_{BrO+NO_2} is $1.7(+0.4 - 0.2)$ larger than given in the JPL-2011 compilation. Our sensitivity study indicates that very likely both σ(BrONO$_2$) and k_{BrO+NO_2} differ from the JPL-2011 recommendation.

The major consequences of our study are threefold. (1) Recent assessments of total stratospheric bromine using the inorganic method during high stratospheric NO_x loadings may have overestimated the necessary correction for the BrO to Br_y ratio. As a consequence, stratospheric [Br_y] should be 1.4 ppt lower, which amounts to 6.8 % of the total stratospheric bromine. (2) A larger J(BrONO$_2$)/k_{BrO+NO_2} ratio may also cause a small increase (maximum -0.8 %) in the bromine-mediated ozone loss in the stratosphere, because ozone loss by BrONO$_2$ and its products is anyhow small. Also an overestimated stratospheric Br_y due to an incorrect J(BrONO$_2$)/k_{BrO+NO_2} ratio would be compensated in the photochemical models, when reactive bromine is calculated using the inorganic method. (3) In the cold troposphere, a diminished formation of BrONO$_2$ where high NO_x meets reactive bromine released from the degradation of organic bromine compounds, or bromine being heterogeneously released from salty aerosols or salt lakes, may lead to a longer lifetime of ozone-destroying BrO. In consequence, the revised J(BrONO$_2$)/k_{BrO+NO_2} ratio may cause more ozone destruction and a more efficient degradation of organic molecules by their reaction with Br atoms on the one hand. On the other hand, it may hinder the activation of reactive bromine tied to the aerosol or in bulk salt at low temperatures (e.g. von Glasow et al., 2004; Salawitch, 2006). Accordingly, the consequences of our finding for ozone, and the oxidation capacity, in the troposphere may largely depend on the specific conditions.

Acknowledgements. This study was funded by the German Ministry of Economy (BMWi) (50EE0840), the European Space Agency (ESA-ESRIN: no. RFQ/3-12092/07/I-OL) and the Deutsche Forschungsgemeinschaft, DFG (grants PF-384/5-1 and 384/5-1 and PF384/9-1/2). Additional funding from the EU projects Reconcile (FP7-ENV-2008-1-226365) and SHIVA (FP7-ENV-2007-1-226224) is highly acknowledged. Furthermore, this work has been supported by the StratPolété project, funded by the French Agence Nationale de la Recherche (ANR-BLAN08-1 31627), the Centre National d'Etudes Spatiales (CNES), the ETHER CNES-INSU database and the Institut Polaire Paul-Emile Victor (IPEV). The SLIMCAT modelling was supported by the NERC National Centre for Atmospheric Science (NCAS), UK. We thank the CNES equipe nacelles pointées and the balloon team from Aire sur l'Adour/France without which the balloon flight would not have been possible. We also thank our colleagues from the LPMA balloon team (P. Jeseck, I. Pepin and Y. Té) for the successful

cooperation. Finally we are grateful for the hospitality and support given by the personnel of Esrange/Kiruna to successfully perform the balloon flight.

Edited by: W. T. Sturges

References

Aliwell, S., Van Roozendael, M., Johnston, P., Richter, A., Wagner, T., Arlander, D., Burrows, J., Fish, D., Jones, R., Tornkvist, K., Lambert, J.-C., Pfeisticker, K., and Pundt, I.: Analysis for BrO in zenith-sky spectra: an intercomparison exercise for analysis improvement, J. Geophys. Res., 107, 4199, doi:10.1029/2001JD000329, 2002.

Bösch, H., Camy-Peyret, C., Chipperfield, M. P., Fitzenberger, R., Harder, H., Schiller, C., Schneider, M., Trautmann, T., and Pfeilsticker, K.: Comparison of measured and modeled startospheric UV/visible actinic fluxes at large solar zenith angles, Geophys. Res. Lett., 28, 1179–1182, 2001.

Bösch, H., Camy-Peyret, C., Chipperfield, M. P., Fitzenberger, R., Harder, H., Platt, U., and Pfeilsticker, K.: Upper limits of stratospheric IO and OIO inferred from center-to-limb-darkening-corrected balloon-borne solar occultation visible spectra: implications for total gaseous iodine and stratospheric ozone, J. Geophys. Res., 108, 4455, doi:10.1029/2002JD003078, 2003.

Brinckmann, S., Engel, A., Bönisch, H., Quack, B., and Atlas, E.: Short-lived brominated hydrocarbons – observations in the source regions and the tropical tropopause layer, Atmos. Chem. Phys., 12, 1213–1228, doi:10.5194/acp-12-1213-2012, 2012.

Butz, A., Bösch, H., Camy-Peyret, C., Chipperfield, M., Dorf, M., Dufour, G., Grunow, K., Jeseck, P., Kühl, S., Payan, S., Pepin, I., Pukite, J., Rozanov, A., von Savigny, C., Sioris, C., Wagner, T., Weidner, F., and Pfeilsticker, K.: Inter-comparison of stratospheric O_3 and NO_2 abundances retrieved from balloon borne direct sun observations and Envisat/SCIAMACHY limb measurements, Atmos. Chem. Phys., 6, 1293–1314, doi:10.5194/acp-6-1293-2006, 2006.

Camy-Peyret, C., Jeseck, P., Payan, S., Hawat, T., Durry, G., and Flaud, J.-M.: Comparison of CH_4 and N_2O profiles at high and mid-latitudes using the LPMA balloon borne Fourier Transform instrument, in: Air Pollution Research Report, Polar Stratospheric Ozone Symposium, Schliersee, 1995.

Chipperfield, M. P.: Multiannual simulations with a three-dimensional chemical transport model, J. Geophys. Res., 104, 1781–1805, 1999.

Chipperfield, M. P.: New version of the TOMCAT/SLIMCAT off-line chemical transport model: intercomparison of stratospheric tracer experiments, Q. J. Roy. Meteorol. Soc., 132, 1179–1203, 2006.

Deutschmann, T., Beirle, S., Frieß, U., Grzegorski, M., Kern, C., Kritten, L., Platt, U., Puķīte, J., Wagner, T., Werner, B., and Pfeilsticker, K.: The Monte Carlo atmospheric radiative transfer model McArtim: introduction and validation of Jacobians and 3D features, J. Quant. Spectrosc. Ra., 112, 1119–1137, 2011.

Dorf, M., Bösch, H., Butz, A., Camy-Peyret, C., Chipperfield, M. P., Engel, A., Goutail, F., Grunow, K., Hendrick, F., Hrechanyy, S., Naujokat, B., Pommereau, J. P., Van Roozendael, M., Sioris, C., Stroh, F., Weidner, F., and Pfeilsticker, K.: Balloon-borne stratospheric BrO measurements: comparison with Envisat/SCIAMACHY BrO limb profiles, Atmos. Chem. Phys., 6, 2483–2501, doi:10.5194/acp-6-2483-2006, 2006a.

Dorf, M., Butler, J., Butz, A., Camy-Peyret, C., Chipperfield, M., Kritten, L., Montzka, S., Simmes, B., Weidner, F., and Pfeilsticker, K.: Long-term observations of stratospheric bromine reveal slow down in growth, Geophys. Res. Lett, 33, L24803, doi:10.1029/2006GL027714, 2006b.

Dorf, M., Butz, A., Camy-Peyret, C., Chipperfield, M. P., Kritten, L., and Pfeilsticker, K.: Bromine in the tropical troposphere and stratosphere as derived from balloon-borne BrO observations, Atmos. Chem. Phys., 8, 7265–7271, doi:10.5194/acp-8-7265-2008, 2008.

Erle, F., Grendel A., Perner D., Platt, U., and Pfeilsticker, K.: Evidence of heterogeneous bromine chemistry on cold stratospheric sulphate aerosols, Geophys. Res. Lett., 25, 23, 4329-4332, 1998.

Feng, W., Chipperfield, M., Davies, S., von der Gathen, S., Kyro, E., Volk, C., Ulanovsky, A., and Belyaev, G.: Large chemical ozone loss in 2004/05 Arctic Winter/Spring, Geophys. Res. Lett., 34, L09803, doi:10.1029/2006GL029098, 2007.

Ferlemann, F., Bauer, N., Fitzenberger, R., Harder, H., Osterkamp, H., Perner, D., Platt, U., Scheider, M., Vradelis, P., and Pfeilsticker, K.: Differential optical absorption spectroscopy instrument for stratospheric balloon-borne trace gas studies, Appl. Opt., 39, 2377–2386, 2000.

Gurlit, W., Bösch, H., Bovensmann, H., Burrows, J. P., Butz, A., Camy-Peyret, C., Dorf, M., Gerilowski, K., Lindner, A., Noël, S., Platt, U., Weidner, F., and Pfeilsticker, K.: The UV-A and visible solar irradiance spectrum: inter-comparison of absolutely calibrated, spectrally medium resolution solar irradiance spectra from balloon- and satellite-borne measurements, Atmos. Chem. Phys., 5, 1879–1890, doi:10.5194/acp-5-1879-2005, 2005.

Harder, H., Camy-Peyret, C., Ferlemann, F., Fitzenberger, R., Hawat, T., Osterkamp, H., Schneider, M., Perner, D., Platt, U., Vradelis, P., and Pfeilsticker, K.: Stratospheric BrO profiles measured at different latitudes and seasons: atmospheric observations, Geophys. Res. Lett., 25, 3843–3846, 1998.

Harder, H., Bösch, H., Camy-Peyret, C., Chipperfield, M., Fitzenberger, R., Payan, S., Perner, D., Platt, U., Sinnhuber, B.-M., and Pfeilsticker, K.: Comparison of measured and modeled Stratospheric BrO: implications for the total amount of stratospheric bromine, Geophys. Res. Lett., 27, 3695–3698, 2000.

Kritten, L., Butz, A., Dorf, M., Deutschmann, T., Kühl, S., Prados-Roman, C., Puķīte, J., Rozanov, A., Schofield, R., and Pfeilsticker, K.: Time dependent profile retrieval of UV/vis absorbing radicals from balloon-borne limb measurements – a case study on NO_2 and O_3, Atmos. Meas. Tech., 3, 933–946, doi:10.5194/amt-3-933-2010, 2010.

Laube, J. C., Engel, A., Bönisch, H., Möbius, T., Worton, D. R., Sturges, W. T., Grunow, K., and Schmidt, U.: Contribution of very short-lived organic substances to stratospheric chlorine and bromine in the tropics – a case study, Atmos. Chem. Phys., 8, 7325–7334, doi:10.5194/acp-8-7325-2008, 2008.

Payan, S., Camy-Peyret, C., Jeseck, P., Hawat, T., Durry, G., and Lefèvre, F.: First direct simultaneous HCl and $ClONO_2$ profile measurements in the artic vortex, Geophys. Res. Lett., 25, 2663–2666, 1998.

Platt, U. and Stutz, J.: Differential Optical Absorption Spectroscopy (DOAS), Principle and Applications, ISBN 3-340-

21193-4, Springer Verlag, Heidelberg, 2008.

Salawitch, R.: Atmospheric chemistry: biogenic bromine, Nature, 439, 275–277, 2006.

Sander, S., Friedl, R. R., Barkern, J., Golden, D., Kurylo, M., Wine, P., Abbat, J., Burkholder, J., Moortgart, C., Huie, R., and Orkin, R. E.: Chemical kinetics and photochemical data for use in atmospheric studies, Technical Report, NASA/JPL Publication, 17, 2011.

Sinnhuber, B.-M., Rozanov, A., Sheode, N., Afe, O. T., Richter, A., Sinnhuber, M., Wittrock, F., Burrows, J. P., Stiller, G. P., von Clarmann, T., and Linden, A.: Global observations of stratospheric bromine monoxide from SCIAMACHY, Geophys. Res. Lett., 32, 1–5, 2005.

Sinnhuber, B.-M., Sheode, N., Sinnhuber, M., Chipperfield, M. P., and Feng, W.: The contribution of anthropogenic bromine emissions to past stratospheric ozone trends: a modelling study, Atmos. Chem. Phys., 9, 2863–2871, doi:10.5194/acp-9-2863-2009, 2009.

Soller, R., Nicovich, J., and Wine, P.: Bromine nitrate photochemistry: quantum yields for O, Br, and BrO over the wavelength range 248–355 nm, J. Phys. Chem. A, 106, 8378–8385, 2002.

Spencer, J. E. and Rowland, F. S.: Bromine nitrate and its stratospheric significance, J. Phys. Chem., 82, 7–10, 1977.

von Glasow, R., von Kuhlmann, R., Lawrence, M. G., Platt, U., and Crutzen, P. J.: Impact of reactive bromine chemistry in the troposphere, Atmos. Chem. Phys., 4, 2481–2497, doi:10.5194/acp-4-2481-2004, 2004.

Weidner, F., Bösch, H., Bovensmann, H., Burrows, J. P., Butz, A., Camy-Peyret, C., Dorf, M., Gerilowski, K., Gurlit, W., Platt, U., von Friedeburg, C., Wagner, T., and Pfeilsticker, K.: Balloon-borne limb profiling of UV/vis skylight radiances, O_3, NO_2, and BrO: technical set-up and validation of the method, Atmos. Chem. Phys., 5, 1409–1422, doi:10.5194/acp-5-1409-2005, 2005.